



# Origin of forbidden reflections in multiferroic $\text{Ba}_2\text{CoGe}_2\text{O}_7$ by neutron diffraction: symmetry lowering or Renninger effect?

Andrew Sazonov,<sup>a,\*</sup> Martin Meven,<sup>a</sup> Georg Roth,<sup>b</sup> Robert Georgii,<sup>c</sup> István Kézsmárki,<sup>d</sup> Vilmos Kocsis,<sup>e,d</sup> Yusuke Tokunaga,<sup>e,f</sup> Yasujiro Taguchi,<sup>e</sup> Yoshinori Tokura<sup>e,g,h</sup> and Vladimir Hutanu<sup>a</sup>

Received 19 October 2015

Accepted 8 February 2016

Edited by G. Kostorz, ETH Zurich, Switzerland

**Keywords:** multiferroic melilite; single-crystal neutron diffraction; multiple diffraction; Renninger effect; *UMWEG*.

**Supporting information:** this article has supporting information at journals.iucr.org/j

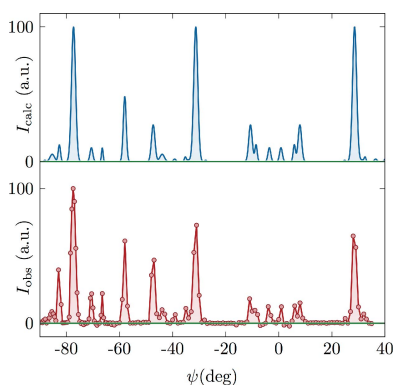
<sup>a</sup>Institute of Crystallography, RWTH Aachen University, and Jülich Centre for Neutron Science (JCNS) at Heinz Maier-Leibnitz Zentrum, 85747 Garching, Germany, <sup>b</sup>Institute of Crystallography, RWTH Aachen University, 52056 Aachen, Germany, <sup>c</sup>Heinz Maier-Leibnitz Zentrum (MLZ) and Physics Department E21, Technical University of Munich, 85747 Garching, Germany, <sup>d</sup>Department of Physics, Budapest University of Technology and Economics, and MTA-BME Lendület Magneto-optical Spectroscopy Research Group, 1111 Budapest, Hungary, <sup>e</sup>RIKEN Center for Emergent Matter Science (CEMS), Wako, Saitama 351-0198, Japan, <sup>f</sup>Department of Advanced Materials Science, University of Tokyo, Kashiwa 277-8561, Japan, <sup>g</sup>Quantum-Phase Electronics Center, Department of Applied Physics, University of Tokyo, Tokyo 113-8656, Japan, and <sup>h</sup>Department of Applied Physics, University of Tokyo, Hongo, Tokyo 113-8656, Japan.  
 \*Correspondence e-mail: mail@sazonov.org

For a symmetry-consistent theoretical description of the multiferroic phase of  $\text{Ba}_2\text{CoGe}_2\text{O}_7$  a precise knowledge of its crystal structure is a prerequisite. In a previous synchrotron X-ray diffraction experiment on multiferroic  $\text{Ba}_2\text{CoGe}_2\text{O}_7$  at room temperature, forbidden reflections were found that favour the tetragonal-to-orthorhombic symmetry lowering of the compound [Hutanu, Sazonov, Murakawa, Tokura, Náfrádi & Chernyshov (2011), *Phys. Rev. B*, **84**, 212101]. Here, the results are reported of room-temperature single-crystal diffraction studies with both hot and cold neutrons to differentiate between genuine symmetry lowering and multiple diffraction (the Renninger effect). A comparison of the experimental multiple diffraction patterns with simulated ones rules out symmetry lowering. Thus, the structural model based on the tetragonal space group  $P\bar{4}_21m$  was selected to describe the  $\text{Ba}_2\text{CoGe}_2\text{O}_7$  symmetry at room temperature. The precise structural parameters from neutron diffraction at 300 K are presented and compared with the previous X-ray diffraction results.

## 1. Introduction

Recently, multiferroic behaviour and static magnetoelectric effects have been observed in many members of the melilite family, e.g.  $\text{Ca}_2\text{CoSi}_2\text{O}_7$ ,  $\text{Sr}_2\text{CoSi}_2\text{O}_7$ ,  $\text{Ba}_2\text{MnGe}_2\text{O}_7$  and  $\text{Ba}_2\text{CoGe}_2\text{O}_7$  [see e.g. Murakawa *et al.* (2012), and references therein]. The dynamic magnetoelectric effect, also observed in these compounds, drastically changes the optical properties of multiferroics compared with conventional materials. For instance, recent work by Kézsmárki *et al.* (2014) discovered quadrochromism at the magnetoelectric spin excitations of multiferroic  $\text{Ca}_2\text{CoSi}_2\text{O}_7$ ,  $\text{Sr}_2\text{CoSi}_2\text{O}_7$  and  $\text{Ba}_2\text{CoGe}_2\text{O}_7$ .

Owing to the lack of complete structural phase diagrams in the case of melilites, the high-symmetry melilite phase is often used as a basis for theoretical calculations and experimental investigations [see e.g. Kézsmárki *et al.* (2014), Szaller *et al.* (2014), Bordács *et al.* (2012), Akaki *et al.* (2009), and references therein]. However, the melilite family shows a variety of structural phase transitions, including incommensurate phases, depending on temperature and chemical composition [see e.g. Jia *et al.* (2006), Kusaka *et al.* (2001), Adams *et al.* (1996), and references therein]. Knowledge of the precise crystal structure



is a very important input for understanding magnetoelectric phenomena in multiferroics. For instance, in the work of Perez-Mato & Ribeiro (2011), the main features of the magnetoelectric behaviour in  $\text{Ba}_2\text{CoGe}_2\text{O}_7$  were predicted by symmetry considerations without referring to any specific microscopic mechanism. Thus, the exact structural model is often an essential starting point for further theoretical and experimental research.

The results of our previous synchrotron X-ray diffraction study on  $\text{Ba}_2\text{CoGe}_2\text{O}_7$  at room temperature and below (Hutaniu *et al.*, 2011) are in accordance with a symmetry lowering from the high-temperature tetragonal structure with space group  $P\bar{4}2_1m$  to the orthorhombic space group  $Cmm2$ . The assumption of the symmetry reduction was based on both the presence of reflections forbidden in  $P\bar{4}2_1m$  (Hutaniu *et al.*, 2011) and the observed magnetic space group  $Cm'm2'$  (Hutaniu *et al.*, 2012). The magnetic space group was then confirmed independently (Hutaniu *et al.*, 2014) by polarized neutron diffraction, namely the spherical neutron polarimetry technique. In contrast, the origin of the observed superstructure reflections in  $\text{Ba}_2\text{CoGe}_2\text{O}_7$  was never cross-checked by other methods. An observation of the weak but well noticeable intensities at the positions of the forbidden reflections in reciprocal space for other melilite compounds, such as  $\text{Ca}_2\text{CoSi}_2\text{O}_7$  (Sazonov *et al.*, 2016) and  $\text{Ba}_2\text{MnGe}_2\text{O}_7$  (Sazonov *et al.*, 2015), motivated us to re-investigate this effect more precisely.

In order to differentiate between genuine symmetry lowering and multiple diffraction or the Renninger effect [see *e.g.* Renninger (1937), Rossmannith (2006), and references therein], neutron diffraction with both short (hot neutrons) and long (cold neutrons) wavelengths was applied. Multiple diffraction patterns (the so-called  $\psi$  scans) were simulated before the experiment in order to select the most appropriate wavelength and positions in reciprocal space. It was found that the scattered intensities detected at the positions of the forbidden reflections are entirely due to multiple diffraction. Thus, the crystal structure of  $\text{Ba}_2\text{CoGe}_2\text{O}_7$  at room temperature can be perfectly described by the tetragonal space group  $P\bar{4}2_1m$ . We present here the results of the model selection based on the multiple diffraction patterns, as well as the complete structure refinement of  $\text{Ba}_2\text{CoGe}_2\text{O}_7$  at room temperature using neutron diffraction.

## 2. Experimental

Single crystals of  $\text{Ba}_2\text{CoGe}_2\text{O}_7$  were grown by the floating-zone technique and were well characterized in previous studies [see Hutaniu *et al.* (2014), and references therein]. The sample used for the neutron diffraction experiment had a cylindrical shape of approximately 6 mm in height and about the same diameter.

Single-crystal neutron diffraction studies with both short and long wavelengths were performed on the two diffractometers HEiDi (Meven & Sazonov, 2015) and MIRA (Georgii & Seemann, 2015) at the FRM II reactor, Heinz Maier-Leibnitz Zentrum, Germany. On HEiDi, the wavelength  $\lambda =$

**Table 1**

Experimental and refinement details from single-crystal neutron diffraction.

Crystal data	
Chemical formula	$\text{Ba}_2\text{CoGe}_2\text{O}_7$
$M_r$	590.81
Cell setting, space group	Tetragonal, $P\bar{4}2_1m$
Temperature (K)	300
$a, c$ (Å)	8.392 (1), 5.561 (1)
$V$ (Å <sup>3</sup> )	391.64 (12)
$Z$	2
$D_x$ (Mg m <sup>-3</sup> )	4.8877
Radiation type	Constant-wavelength neutron diffraction radiation, $\lambda = 0.793$ Å
$\mu$ (mm <sup>-1</sup> )	0.01
Crystal form, colour	Cylinder, dark blue
Crystal size (mm)	6 × 3 (radius)
Data collection	
Diffractometer	Four-circle diffractometer HEiDi†
Radiation source	Nuclear reactor
Monochromator	Ge(422)
Temperature (K)	300
Data collection method	$\omega$ scans
$\theta_{\text{max}}$ (°)	49.45
$[\sin\theta/\lambda]_{\text{max}}$ (Å <sup>-1</sup> )	0.96
Range of $h, k, l$	0 → $h$ → 16 0 → $k$ → 16 -10 → $l$ → 10
No. of measured reflections	1750
No. of independent reflections	555
No. of independent reflections with $I > 3\sigma(I)$	554
$R_{\text{int}}$	0.024
Refinement	
Refinement on	$F^2$
$R[F^2 > 3\sigma(F^2)]$ , $wR(F^2)$ , $S$	0.028, 0.043, 1.73
No. of reflections	555
No. of parameters	35
Weighting scheme, $w$	$1/[\sigma^2(I) + 0.0004I^2]$
Extinction correction	Isotropic, Lorentzian type 1‡
Extinction coefficient	0.242 (7)

† See Meven & Sazonov (2015). ‡ According to Becker & Coppens (1974).

0.793 Å was obtained from a Ge(422) monochromator with an Er filter used to suppress the  $\lambda/2$  contamination. A <sup>3</sup>He point detector, optimized for neutrons of short wavelength, was used for the measurement of  $\psi$  scans and a full data collection at room temperature. On MIRA, the wavelength  $\lambda = 4.488$  Å was obtained from a highly oriented pyrolytic graphite monochromator with a Be filter to suppress the  $\lambda/2$  contamination. Both point and position-sensitive detectors were used for the measurement of  $\psi$  scans at room temperature.

On both instruments, an Eulerian cradle was used and the sample was oriented in such a way as to have the forbidden reflections of  $h00$  type in the scattering plane when the  $\chi$  angle in the conventional four-cycle geometry was approximately 90°. This geometry allows an easy rotation around  $\psi$  by 360° as it almost coincides with the conventional  $\varphi$  rotation. As the first step of the measurements, the orientation matrix was refined. Secondly, the conventional  $\theta$ ,  $\omega$ ,  $\chi$  and  $\varphi$  values for any of the requested  $\psi$  angles were calculated by the data collection program *DIF4* for HEiDi. Then, an  $\omega$  scan was performed for each  $\psi$  value and the integrated intensity of the scan was assigned to that  $\psi$  point. As a result, a curve of the

integrated intensity *versus*  $\psi$  was obtained, which was further compared with the calculations of possible multiple diffraction.

The integrated intensities of the reflections collected with the point detector were obtained using the *DAVINCI* program (Sazonov, 2015). The multiple diffraction patterns were simulated using the *UMWEG* program (Rossmannith, 2003). The structural parameters of  $\text{Ba}_2\text{CoGe}_2\text{O}_7$  were refined from the full data collection using the *JANA2006* program (Petříček *et al.*, 2014). Experimental and refinement details are summarized in Table 1.

### 3. Results and discussion

#### 3.1. Room-temperature crystal structure model

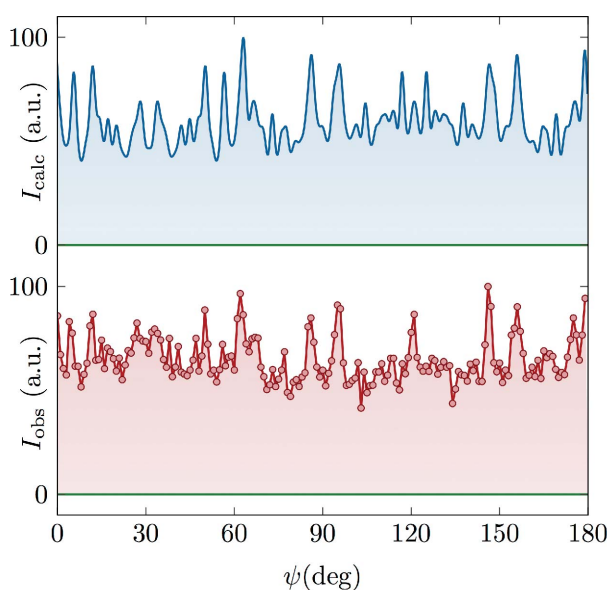
In single-crystal neutron diffraction studies performed with short wavelengths ( $\lambda \lesssim 1.2 \text{ \AA}$ ) on melilite compounds, we have often observed weak reflections at the positions of reflections forbidden in the tetragonal space group  $P4_2m$ . The intensities of those reflections are usually more than three times their standard deviations ( $3\sigma$ ) and, in general, could be explained by higher-order wavelength contamination, multiple diffraction or symmetry lowering.

However, the forbidden reflections are found to be much stronger than possible contaminations by higher-order wavelengths, which are effectively suppressed by the specific filters. Thus, at the HEiDi diffractometer with  $\lambda = 0.793 \text{ \AA}$ , the  $\lambda/2$  contribution is expected to be less than 0.5%. In contrast, the experimentally measured intensities are much stronger and reach up to a few percent. Therefore, higher-order wavelength contamination is excluded from the list of possible explanations of the observed superstructure reflections.

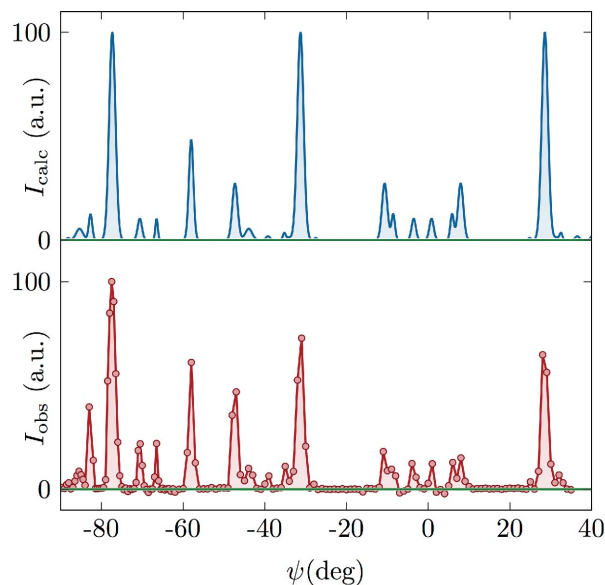
In order to study the influence of the possible multiple diffraction contribution in  $\text{Ba}_2\text{CoGe}_2\text{O}_7$ , a simulation of the  $\psi$  scans was performed prior to the experiment. The instrumental parameters used in the simulation are the horizontal and vertical beam divergences ( $\delta_H, \delta_V$ ) and the wavelength spread ( $\Delta\lambda/\lambda$ ) of the incident beam. These were estimated from the geometry of the instrument. The  $\text{Ba}_2\text{CoGe}_2\text{O}_7$  sample-specific parameters, like the mosaic spread ( $\nu$ ) and the mosaic block radius ( $r$ ), were set manually. Fractional atomic coordinates ( $x, y, z$ ) and anisotropic atomic displacement parameters ( $U_{\text{aniso}}$ ) for  $\text{Ba}_2\text{CoGe}_2\text{O}_7$  were obtained from the structure refinement using the present single-crystal neutron diffraction data (see next section).

Fig. 1 shows a comparison of the simulated multiple diffraction pattern for the forbidden 300 reflection and the experimental data collected at HEiDi with  $\lambda = 0.793 \text{ \AA}$ . The following parameters were used in the calculations:  $\Delta\lambda/\lambda = 0.01, \delta_H = 0.7^\circ, \delta_V = 1.6^\circ, r = 15 \text{ \mu m}$  and  $\nu = 0^\circ$ . Good agreement between the calculated and experimental data indicates that both instrumental and sample-specific parameters were reasonably selected. As can be seen from Fig. 1, the very broad peaks on the  $\psi$  scan make it impossible to separate the case of symmetry lowering from that of multiple diffraction. There is no single point in the diffraction pattern without an overlap of neighbouring reflections and the intensity never drops down to zero. As a result, the possible contribution caused by symmetry reduction could be well hidden by the multiple diffraction part. A comparison of the simulated and experimental intensities is not reliable and therefore could not be used to solve the problem.

In contrast with the short-wavelength case, cold neutrons make it possible to overcome the problem with overlapping peaks in the  $\psi$  scans. A change of just one single parameter,



**Figure 1** Multiple diffraction pattern of the forbidden 300 reflection of  $\text{Ba}_2\text{CoGe}_2\text{O}_7$  according to calculation (top, blue curve) and the single-crystal neutron diffraction experiment (bottom, red curve) with a short wavelength  $\lambda = 0.793 \text{ \AA}$ .



**Figure 2** Multiple diffraction pattern of the forbidden 100 reflection of  $\text{Ba}_2\text{CoGe}_2\text{O}_7$  according to calculation (top, blue curve) and the single-crystal neutron diffraction experiment (bottom, red curve) with a long wavelength  $\lambda = 4.488 \text{ \AA}$ .

**Table 2**

Fractional atomic coordinates ( $x, y, z$ ) and isotropic atomic displacement parameters  $U_{\text{iso}}$  ( $\text{\AA}^2$ ) for  $\text{Ba}_2\text{CoGe}_2\text{O}_7$  refined in space group  $P\bar{4}2_1m$  according to the present single-crystal neutron diffraction data at 300 K.

Ion	Wyckoff position	$x$	$y$	$z$	$U_{\text{iso}}$
Ba	4e	0.33479 (7)	0.16521 (7)	0.49267 (17)	0.00731 (12)
Co	2b	0	0	0	0.00630 (30)
Ge	4e	0.14053 (5)	0.35947 (5)	0.03986 (10)	0.00520 (10)
O1	2c	0	0.5	0.15810 (20)	0.00968 (18)
O2	4e	0.13843 (8)	0.36157 (8)	0.72982 (15)	0.01017 (12)
O3	8f	0.07949 (9)	0.18468 (7)	0.18715 (14)	0.00997 (12)

the wavelength  $\lambda$ , in the simulation process from  $\lambda = 0.793 \text{ \AA}$  to  $\lambda = 4.488 \text{ \AA}$  drastically modifies the entire multiple diffraction pattern. The number of peaks is reduced and they become well separated from each other. Regions of zero intensity appear on the simulated curve. An adjustment of the instrumental parameters allows us to achieve better agreement between the experimental data and calculations. Thus, in the simulations with cold neutrons, the following parameters were used:  $\Delta\lambda/\lambda = 0.01$ ,  $\delta_{\text{H}} = 0.5^\circ$ ,  $\delta_{\text{V}} = 0.5^\circ$ ,  $r = 15 \text{ \mu m}$  and  $\nu = 0^\circ$ . We selected the forbidden 100 reflection for the measurement because the 300 reflection was not reachable with the long wavelength. The experimental values for 100 agree well with the calculation, as can be seen in Fig. 2. We were able to reproduce the zero-intensity regions experimentally. Therefore, the observed intensity at the positions of the forbidden reflections could be explained solely by multiple diffraction. This rules out the symmetry lowering scenario in  $\text{Ba}_2\text{CoGe}_2\text{O}_7$  and supports the tetragonal space group  $P\bar{4}2_1m$  as the correct description of the true structure at room temperature.

However, the question about the symmetry of  $\text{Ba}_2\text{CoGe}_2\text{O}_7$  in the antiferromagnetic state (below  $T_{\text{N}} \simeq 6.7 \text{ K}$ ) remains open. In the magnetically ordered state at low temperatures, a separation between the symmetry lowering and multiple diffraction cases becomes much more difficult because of the allowed magnetic contribution to the positions of the forbidden reflections on the  $\psi$  scans (due to the extinction rules). In that case, the use of polarized neutron diffraction is preferable, which could allow us to separate the nuclear part from the magnetic one. However, the geometric limitations on sample rotation and inclination caused by the necessity of using a cryostat significantly complicate the experimental setup. As a result, the method applied here is not easily applicable to unambiguous determination of the crystal structure at low temperatures.

It should be noted that, in our previous synchrotron X-ray diffraction study on  $\text{Ba}_2\text{CoGe}_2\text{O}_7$  below room temperature, we also observed the forbidden reflections and interpreted them as a symmetry lowering (Hutano *et al.*, 2011). In that experiment, the test  $\psi$  scan did not show a complete disappearance of the intensity at the positions of the forbidden reflections. The instrumental parameters, such as the beam divergence and wavelength spread, are expected to be much smaller for the synchrotron X-ray case and, as a result, the peaks on the  $\psi$  scan should be separated even at short

**Table 3**

Anisotropic atomic displacement parameters  $U_{\text{aniso}}$  ( $\text{\AA}^2$ ) for  $\text{Ba}_2\text{CoGe}_2\text{O}_7$  refined in space group  $P\bar{4}2_1m$  according to the present single-crystal neutron diffraction data at 300 K.

Ion	$U_{11}$	$U_{22}$	$U_{33}$
Ba	0.00743 (18)	$U_{11}$	0.00710 (20)
Co	0.00550 (40)	$U_{11}$	0.00800 (80)
Ge	0.00514 (11)	$U_{11}$	0.00532 (17)
O1	0.01080 (20)	$U_{11}$	0.00740 (40)
O2	0.01205 (19)	$U_{11}$	0.00640 (20)
O3	0.01330 (30)	0.00657 (20)	0.01005 (17)

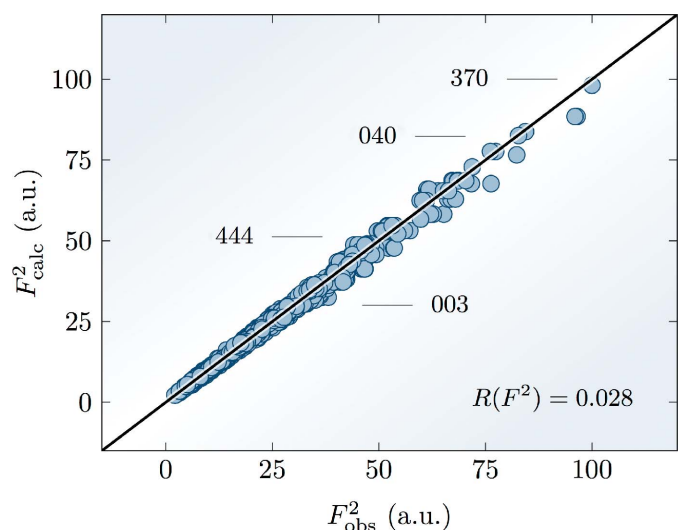
  

Ion	$U_{12}$	$U_{13}$	$U_{23}$
Ba	0.00247 (19)	-0.00058 (16)	$-U_{13}$
Co	0	0	0
Ge	0.00053 (13)	-0.00002 (8)	$-U_{13}$
O1	0.00590 (30)	0	0
O2	0.00230 (30)	0.00043 (14)	$-U_{13}$
O3	-0.00288 (15)	-0.00213 (18)	0.00046 (6)

wavelengths. However, the short wavelength ( $\lambda \simeq 0.7 \text{ \AA}$ ), combined with the possible large mosaicity of the sample used in that experiment, could significantly increase the peak width and thus hide the zero-intensity regions.

### 3.2. Room-temperature structural details

In order to determine the precise structural parameters for  $\text{Ba}_2\text{CoGe}_2\text{O}_7$  at room temperature we performed a refinement of our neutron diffraction data using the crystal structure model selected in the previous section (space group  $P\bar{4}2_1m$ ). The starting parameters were taken from the published structure determined by synchrotron X-ray diffraction at 293 K (Hutano *et al.*, 2011). All atomic positions which are not restricted by symmetry were refined, together with the



**Figure 3** The quality of the  $\text{Ba}_2\text{CoGe}_2\text{O}_7$  crystal structure refinement in space group  $P\bar{4}2_1m$  according to the present single-crystal neutron diffraction data at 300 K. The experimentally measured integrated intensities ( $F_{\text{obs}}^2$ ) are plotted against the calculated ones ( $F_{\text{calc}}^2$ ). The intensities of a few selected Bragg reflections are marked.

anisotropic atomic displacements ( $U_{\text{aniso}}$ ) and the scale and extinction parameters. Note that the intensities of strong reflections may be reduced by multiple diffraction, an effect which is not taken into account in the refinement calculations. The agreement between the experimental and calculated data is shown in Fig. 3. Table 2 presents the refined atomic coordinates and the isotropic atomic displacement ( $U_{\text{iso}}$ ) parameters, while  $U_{\text{aniso}}$  are given in Table 3. Full details of the refinement, including bond lengths and angles, are provided in the deposited crystallographic information file.

A comparison of the room-temperature structure from neutron and synchrotron X-ray diffraction shows a negligible difference in the positional parameters with an average value of less than  $1\sigma$ . The largest shift in the atomic positions, of approximately  $0.007 \text{ \AA}$ , is found for  $z_{\text{O}_2}$ .

## 4. Conclusions

In order to differentiate between genuine symmetry lowering and multiple diffraction (the Renninger effect), single-crystal neutron diffraction experiments with both hot and cold neutrons were performed. It was found that the scattered intensities detected at the positions of the forbidden reflections are entirely due to multiple diffraction. Thus, the crystal structure of  $\text{Ba}_2\text{CoGe}_2\text{O}_7$  at room temperature can be described by the tetragonal space group  $P\bar{4}2_1m$  without any symmetry lowering. The precise structural parameters of  $\text{Ba}_2\text{CoGe}_2\text{O}_7$  at 300 K are found to be in a good agreement with the previous synchrotron X-ray diffraction results.

The same conclusion about the multiple diffraction origin of the forbidden reflections was also reached by Birkenstock *et al.* (2013) for the bismuth metal oxides  $\text{Bi}_2\text{Fe}_4\text{O}_9$  and  $\text{Bi}_2\text{Ga}_4\text{O}_9$  based on single-crystal neutron diffraction with different wavelengths. Thus, there is always a risk of misinterpreting those reflections, especially in experiments with hot neutrons. In order to determine the correct space group during crystal structure analysis, the software *UMWEG* was used, which allows the user to simulate multiple diffraction events and to estimate both instrumental (beam divergences, wavelength spread) and sample-specific (mosaicity) parameters.

## Acknowledgements

We thank Professor G. Heger for fruitful discussions. This work was partly supported by the BMBF under contract No. 05K13PA3 and by the Hungarian Research Fund OTKA K108918. Part of the work is based upon experiments

performed at the HEiDi instrument which is operated by RWTH Aachen/FZ Jülich (Jülich Aachen Research Alliance JARA).

## References

- Adams, R. D., Payen, C. & Datta, T. (1996). *Inorg. Chem.* **35**, 3492–3497.
- Akaki, M., Tozawa, J., Akahoshi, D. & Kuwahara, H. (2009). *Appl. Phys. Lett.* **94**, 212904.
- Becker, P. J. & Coppens, P. (1974). *Acta Cryst.* **A30**, 129–147.
- Birkenstock, J., Nénert, G., Gesing, T. M., Burianek, M., Mühlberg, M. & Fischer, R. X. (2013). *Z. Kristallogr.* **228**, 611–619.
- Bordács, S., Kézsmárki, I., Szaller, D., Demkó, L., Kida, N., Murakawa, H., Onose, Y., Shimano, R., Rődöm, T., Nagel, U., Miyahara, S., Furukawa, N. & Tokura, Y. (2012). *Nat. Phys.* **8**, 734–738.
- Georgii, R. & Seemann, K. (2015). *J. Large-scale Res. Facilities JLSRF*, **1**, A3.
- Hutano, V., Sazonov, A. P., Meven, M., Murakawa, H., Tokura, Y., Bordács, S., Kézsmárki, I. & Náfrádi, B. (2012). *Phys. Rev. B*, **86**, 104401.
- Hutano, V., Sazonov, A. P., Meven, M., Roth, G., Gukasov, A., Murakawa, H., Tokura, Y., Szaller, D., Bordács, S., Kézsmárki, I., Guduru, V. K., Peters, L. C. J. M., Zeitler, U., Romhányi, J. & Náfrádi, B. (2014). *Phys. Rev. B*, **89**, 064403.
- Hutano, V., Sazonov, A. P., Murakawa, H., Tokura, Y., Náfrádi, B. & Chernyshov, D. (2011). *Phys. Rev. B*, **84**, 212101.
- Jia, Z. H., Schaper, A. K., Massa, W., Treutmann, W. & Rager, H. (2006). *Acta Cryst.* **B62**, 547–555.
- Kézsmárki, I., Szaller, D., Bordács, S., Kocsis, V., Tokunaga, Y., Taguchi, Y., Murakawa, H., Tokura, Y., Engelkamp, H., Rődöm, T. & Nagel, U. (2014). *Nat. Commun.* **5**, 1–9.
- Kusaka, K., Hagiya, K., Okano, Y., Mukai, M., Iishi, K., Haga, N. & Ohmasa, M. (2001). *Phys. Chem. Miner.* **28**, 150–166.
- Meven, M. & Sazonov, A. (2015). *J. Large-scale Res. Facilities JLSRF*, **1**, A7.
- Murakawa, H., Onose, Y., Miyahara, S., Furukawa, N. & Tokura, Y. (2012). *Phys. Rev. B*, **85**, 174106.
- Perez-Mato, J. M. & Ribeiro, J. L. (2011). *Acta Cryst.* **A67**, 264–268.
- Petříček, V., Dušek, M. & Palatinus, L. (2014). *Z. Kristallogr.* **229**, 345–352.
- Renninger, M. (1937). *Z. Phys.* **106**, 141–176.
- Rossmannith, E. (2003). *J. Appl. Cryst.* **36**, 1467–1474.
- Rossmannith, E. (2006). *Acta Cryst.* **A62**, 174–177.
- Sazonov, A. P. (2015). *DAVINCI*, <http://sazonov.org/soft.html#davinci>.
- Sazonov, A. P., Hutano, V. & Georgii, R. (2015). Experimental Report 3224. Heinz Maier-Leibnitz Zentrum, Garching, Germany.
- Sazonov, A., Hutano, V., Meven, M., Roth, G., Kézsmárki, I., Murakawa, H., Tokura, Y. & Náfrádi, B. (2016). *Acta Cryst.* **B72**, 126–132.
- Szaller, D., Bordács, S., Kocsis, V., Rődöm, T., Nagel, U. & Kézsmárki, I. (2014). *Phys. Rev. B*, **89**, 184419.